Supporting Information (SI)

Efficient electrocatalytic CO_2 conversion into Formate by $Al_xBi_yO_z$ nanorods in a wide potential window

Zhaoyu Kuang[ab], Chunlei Peng[ab], Chengjin Li[a], Heliang Yao[a], Xiaoxia Zhou*[a] and Hangrong Chen*[ac]

[a]State Key Laboratory of High Performance Ceramics and Superfine Microstructure, Shanghai Institute of Ceramics, Chinese Academy of Sciences, 1295 Dingxi Road, Shanghai 200050 (P.R.China)

[b]Center of Materials Science and Optoelectronics Engineering, University of Chinese Academy of Sciences, Beijing 100049 (P. R. China)

[c]School of Chemistry and Materials Science, Hangzhou Institute for Advanced Study, University of Chinese Academy of Sciences, 1 Sub-lane Xiangshan, Hangzhou 310024 (P. R. China)

*Corresponding author. E-mail: zhouxiaoxia@mail.sic.ac.cn (Xiaoxia Zhou), hrchen@mail.sic.ac.cn (Hangrong Chen)

Supplementary Figures:

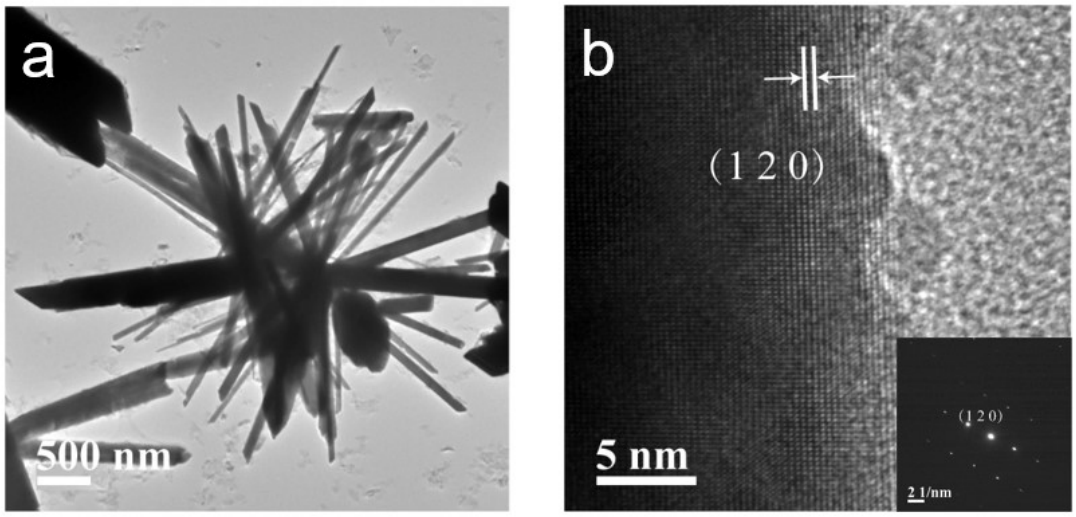

Fig. S1 (a) Typical TEM image, (b) HRTEM image and SAED pattern (inset) of R-Bi_2O_3.

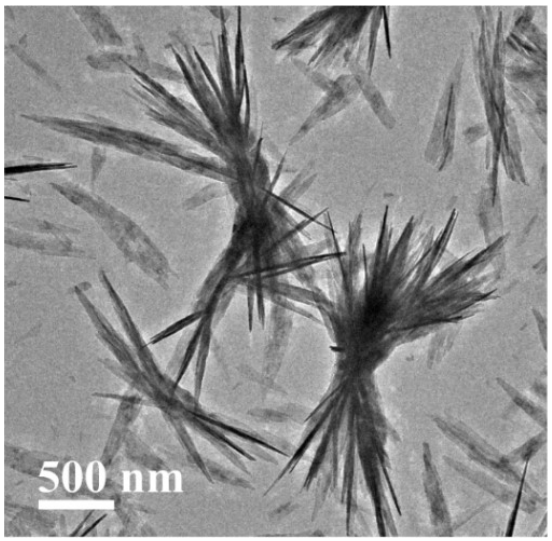

Fig. S2 Typical TEM image of Al_2O_3.

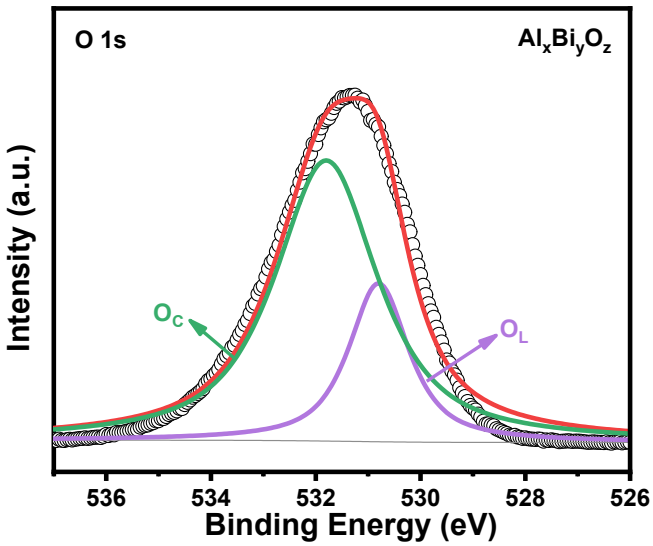

Fig. S3 High-resolution O 1s XPS spectrum of $Al_xBi_yO_z$ nanorods.

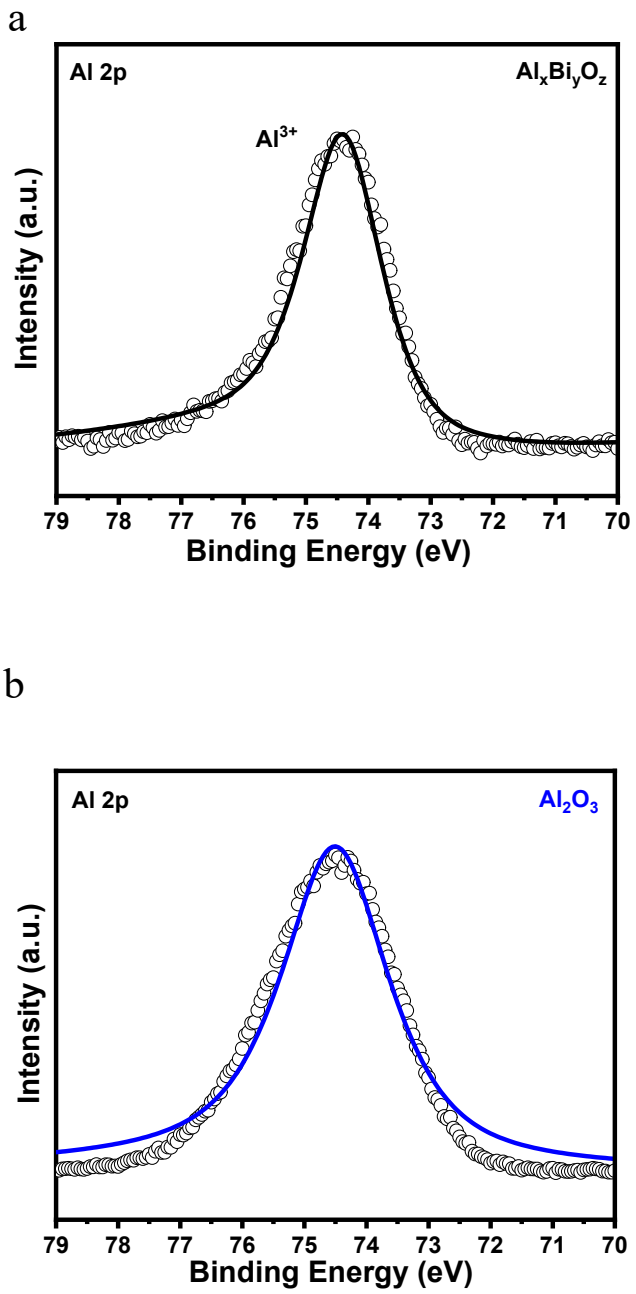

Fig. S4 High-resolution Al 2p XPS spectra of (a) $Al_xBi_yO_z$ nanorods and (b) Al_2O_3.

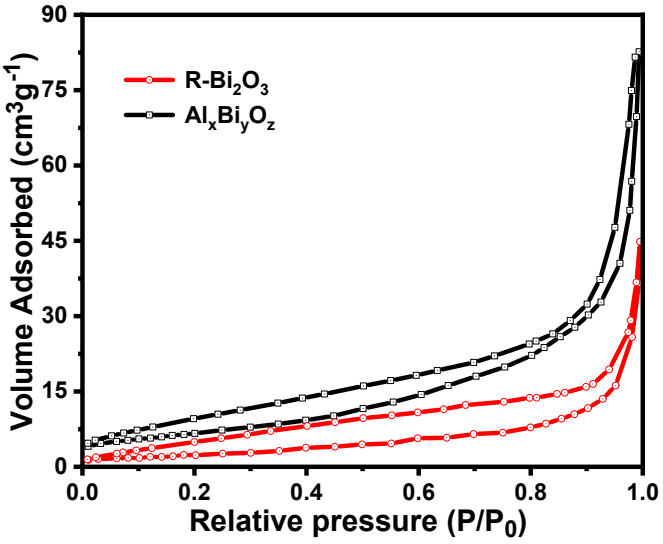

Fig. S5 Nitrogen adsorption-desorption isotherms of $Al_xBi_yO_z$ and R-Bi_2O_3.

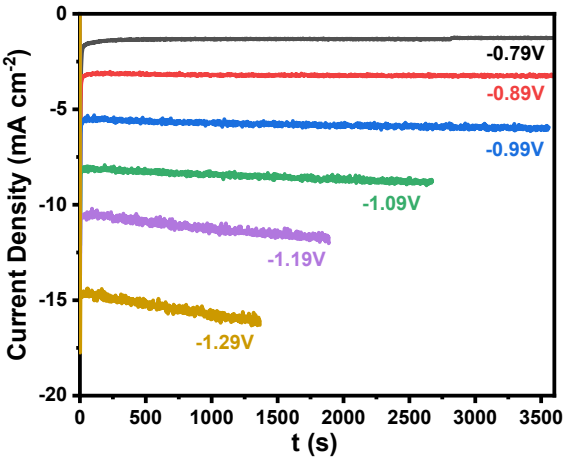

Fig. S6 Current density at six fixed potentials of $Al_xBi_yO_z$ nanorods.

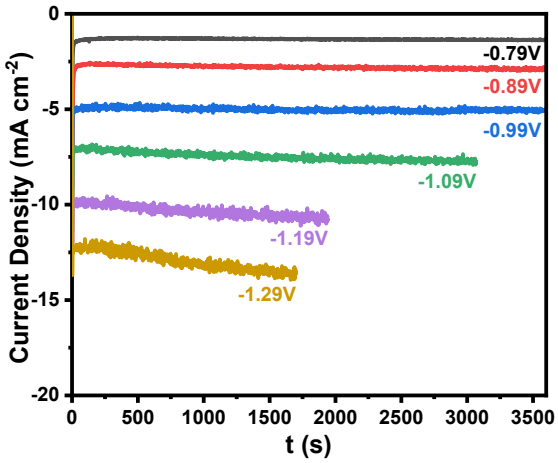

Fig. S7 Current density at six fixed potentials of R-Bi_2O_3.

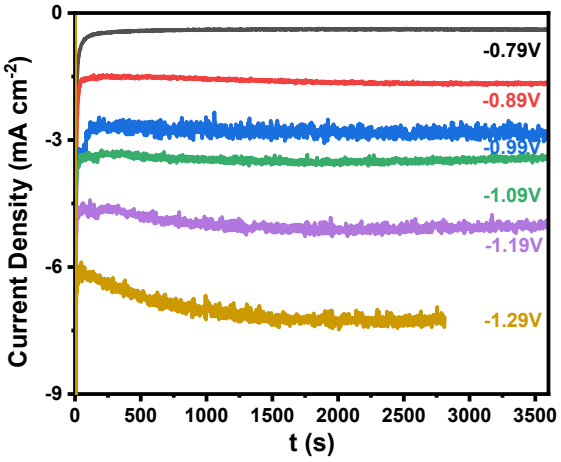

Fig. S8 Current density at six fixed potentials of Al_2O_3.

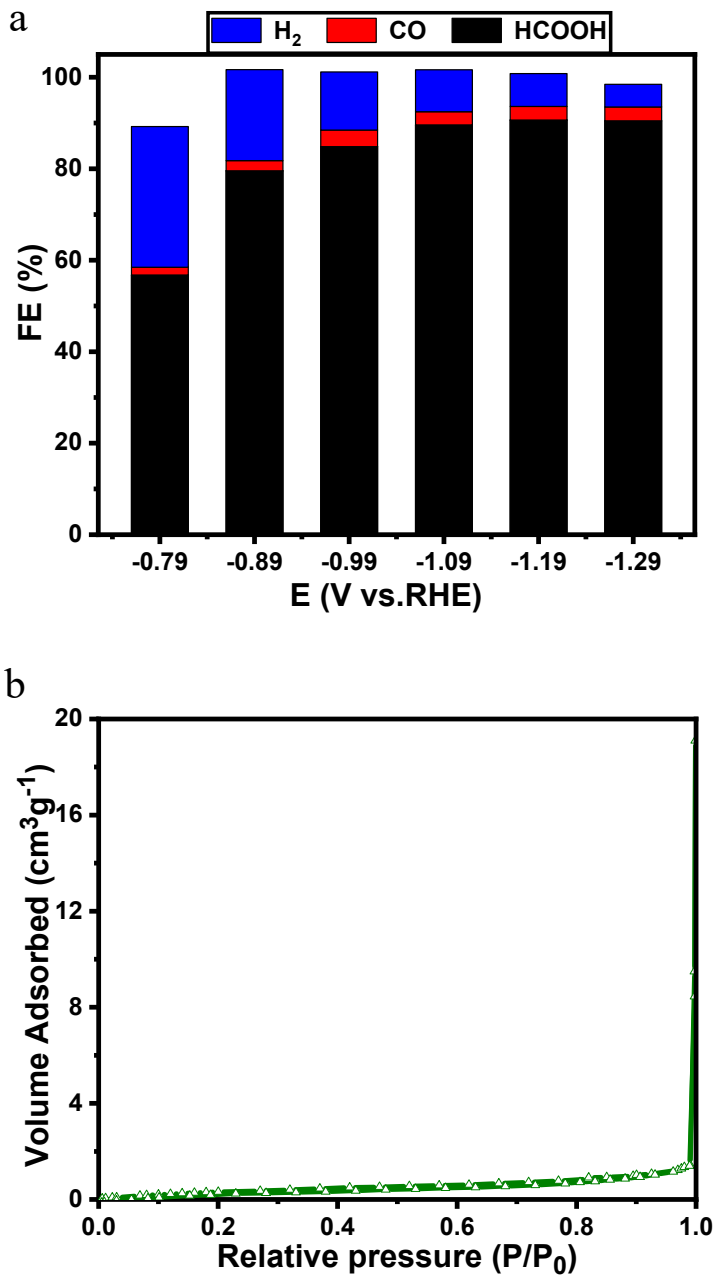

Fig. S9 (a) Faradaic efficiencies at different potentials, (b) Nitrogen adsorption-desorption isotherm of commercial Bi_2O_3.

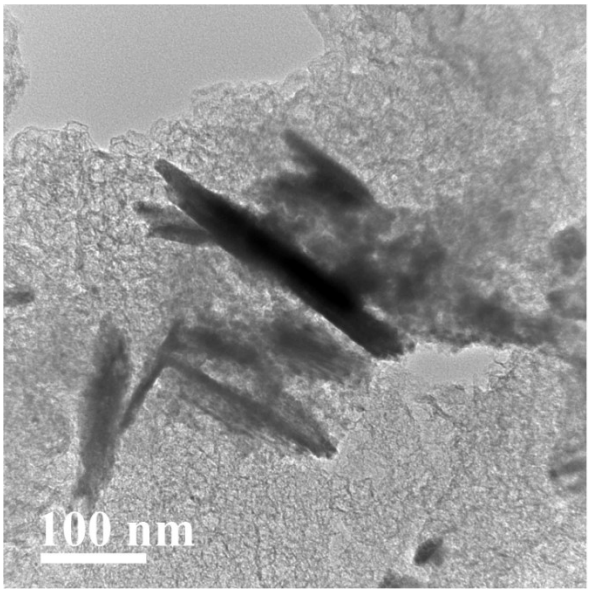

Fig. S10 TEM image of $Al_xBi_yO_z$ after chronoamperometric electrolysis for 10 h.

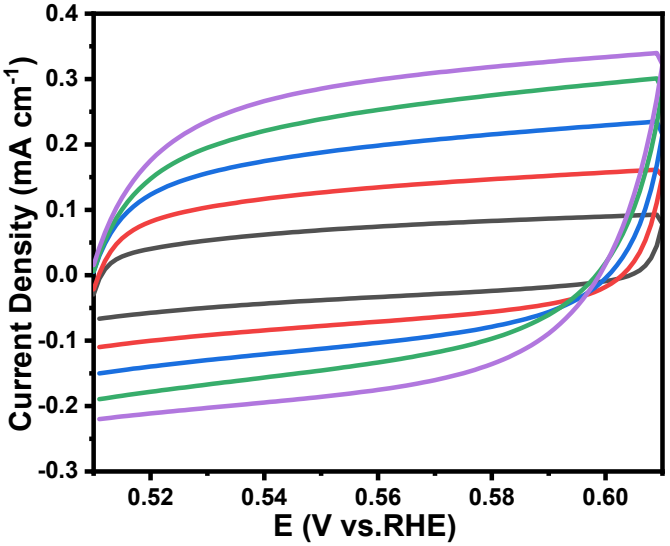

Fig. S11 CV curves at different scan rates of $Al_xBi_yO_z$.

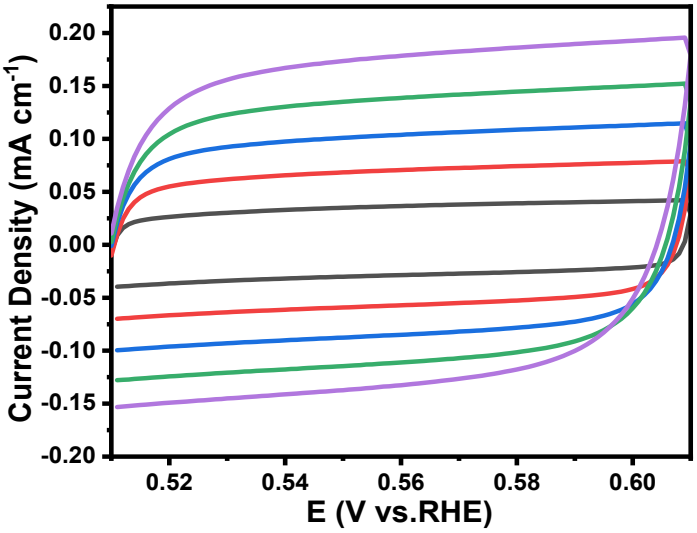

Fig. S12 CV curves at different scan rates of R-Bi_2O_3.

Table. S1 Comparison of the performances between the reported Bi-based catalysts and this work.

Catalyst	Electrolyte	FE_{HCOO-}	Formation rate	Ref
Bi(btb) derived Bi/organic matrix	0.5M $KHCO_3$	67% (-0.77V)	0.1 mmol·$h^{-1}cm^{-1}$ (−0.97 V)	1
Bi-MOF (CAU-17)	0.1M $KHCO_3$	85% (-0.8V)	/	2
Bi/Bi_2O_3 nanosheets	0.5M $KHCO_3$	90.4% (-0.87V)	1.12 mmol·$mg^{-1}h^{-1}cm^{-2}$ (-1.17V)	3
$BiPO_4$ derived Bi/Bi_2O_3 nanosheets	0.5M $KHCO_3$	~75% (-0.8V)	/	4
Bi nanosheets on Ag nanowire	0.5M $KHCO_3$	~90% (-0.8V)	/	5
Bi nanosheets (flow cell)	0.5M $KHCO_3$	91.6% (-0.8V)	/	6
Bi nanoparticles on carbon nanosheets	0.5M $KHCO_3$	86% (-0.83V)	0.46 mmol·$h^{-1}cm^{-1}$ (−0.97 V)	7
Bi nanorods@N-C nanotubes	0.1M $KHCO_3$	~65% (-0.8V)	/	8
$Al_xBi_yO_z$ nanorods	0.1M $KHCO_3$	91.5(-0.79V)	0.1 mmol·$h^{-1}cm^{-1}$ (−0.99 V)	this work

All potentials in this table are measured against the RHE reference.

References

1 P. Lamagni, M. Miola, J. Catalano, M. S. Hvid, M. A. H. Mamakhel, M. Christensen, M. R. Madsen, H. S. Jeppesen, X. M. Hu, K. Daasbjerg, T. Skrydstrup and N. Lock, *Adv. Funct. Mater.*, 2020, **30**, 11.

2 F. Li, G. H. Gu, C. Choi, P. Kolla, S. Hong, T. S. Wu, Y. L. Soo, J. Masa, S. Mukerjee, Y. S. Jung, J. S. Qiu and Z. Y. Sun, *Appl. Catal., B.*, 2020, **277**, 10.

3 D. Wu, G. Huo, W. Y. Chen, X. Z. Fu and J. L. Luo, *Appl. Catal., B.*, 2020, **271**, 8.

4 Y. T. Wang, Y. H. Li, J. Z. Liu, C. X. Dong, C. Q. Xiao, L. Cheng, H. L. Jiang, H. Jiang and C. Z. Li, *Angew. Chem., Int. Ed.*, 2021, **60**, 7681-7685.

5 J. Z. Liu, Y. H. Li, Y. T. Wang, C. Q. Xiao, M. M. Liu, X. D. Zhou, H. Jiang and C. Z. Li, *Nano Res.*, 2021.

6 L. C. Yi, J. X. Chen, P. Shao, J. H. Huang, X. X. Peng, J. W. Li, G. X. Wang, C. Zhang and Z. H. Wen, *Angew. Chem., Int. Ed.*, 2020, **59**, 20112-20119.

7 D. Wu, X. W. Wang, X. Z. Fu and J. L. Luo, *Appl. Catal., B.*, 2021, **284**, 10.

8 W. J. Zhang, S. Y. Yang, M. H. Jiang, Y. Hu, C. Q. Hu, X. L. Zhang and Z. Jin, *Nano Lett.*, 2021, **21**, 2650-2657.